

Observation of the decay $D_s^+ \rightarrow \omega\pi^+\eta$

M. Ablikim¹, M. N. Achasov^{12,b}, P. Adlarson⁷², M. Albrecht⁴, R. Aliberti³³, A. Amoroso^{71A,71C}, M. R. An³⁷, Q. An^{68,55}, Y. Bai⁵⁴, O. Bakina³⁴, R. Baldini Ferroli^{27A}, I. Balossino^{28A}, Y. Ban^{44,g}, V. Batozskaya^{1,42}, D. Becker³³, K. Begzsuren³⁰, N. Berger³³, M. Bertani^{27A}, D. Bettoni^{28A}, F. Bianchi^{71A,71C}, E. Bianco^{71A,71C}, J. Bloms⁶⁵, A. Bortone^{71A,71C}, I. Boyko³⁴, R. A. Briere⁵, A. Brueggemann⁶⁵, H. Cai⁷³, X. Cai^{1,55}, A. Calcaterra^{27A}, G. F. Cao^{1,60}, N. Cao^{1,60}, S. A. Cetin^{59A}, J. F. Chang^{1,55}, W. L. Chang^{1,60}, G. R. Che⁴¹, G. Chelkov^{34,a}, C. Chen⁴¹, Chao Chen⁵², G. Chen¹, H. S. Chen^{1,60}, M. L. Chen^{1,55,60}, S. J. Chen⁴⁰, S. M. Chen⁵⁸, T. Chen^{1,60}, X. R. Chen^{29,60}, X. T. Chen^{1,60}, Y. B. Chen^{1,55}, Z. J. Chen^{24,h}, W. S. Cheng^{71C}, S. K. Choi⁵², X. Chu⁴¹, G. Cibinetto^{28A}, F. Cossio^{71C}, J. J. Cui⁴⁷, H. L. Dai^{1,55}, J. P. Dai⁷⁶, A. Dbeysy¹⁸, R. E. de Boer⁴, D. Dedovich³⁴, Z. Y. Deng¹, A. Denig³³, I. Denysenko³⁴, M. Destefanis^{71A,71C}, F. De Mori^{71A,71C}, Y. Ding³⁸, Y. Ding³², J. Dong^{1,55}, L. Y. Dong^{1,60}, M. Y. Dong^{1,55,60}, X. Dong⁷³, S. X. Du⁷⁸, Z. H. Duan⁴⁰, P. Egorov^{34,a}, Y. L. Fan⁷³, J. Fang^{1,55}, S. S. Fang^{1,60}, W. X. Fang¹, Y. Fang¹, R. Farinelli^{28A}, L. Fava^{71B,71C}, F. Feldbauer⁴, G. Felici^{27A}, C. Q. Feng^{68,55}, J. H. Feng⁵⁶, K. Fischer⁶⁶, M. Fritsch⁴, C. Fritsch⁶⁵, C. D. Fu¹, H. Gao⁶⁰, Y. N. Gao^{44,g}, Yang Gao^{68,55}, S. Garbolino^{71C}, I. Garzia^{28A,28B}, P. T. Ge⁷³, Z. W. Ge⁴⁰, C. Geng⁵⁶, E. M. Gersabeck⁶⁴, A. Gilman⁶⁶, K. Goetzen¹³, L. Gong³⁸, W. X. Gong^{1,55}, W. Gradl³³, M. Greco^{71A,71C}, L. M. Gu⁴⁰, M. H. Gu^{1,55}, Y. T. Gu¹⁵, C. Y. Guan^{1,60}, A. Q. Guo^{29,60}, L. B. Guo³⁹, R. P. Guo⁴⁶, Y. P. Guo^{11,f}, A. Guskov^{34,a}, W. Y. Han³⁷, X. Q. Hao¹⁹, F. A. Harris⁶², K. K. He⁵², K. L. He^{1,60}, F. H. Heinsius⁴, C. H. Heinz³³, Y. K. Heng^{1,55,60}, C. Herold⁵⁷, G. Y. Hou^{1,60}, Y. R. Hou⁶⁰, Z. L. Hou¹, H. M. Hu^{1,60}, J. F. Hu^{53,i}, T. Hu^{1,55,60}, Y. Hu¹, G. S. Huang^{68,55}, K. X. Huang⁵⁶, L. Q. Huang^{29,60}, X. T. Huang⁴⁷, Y. P. Huang¹, Z. Huang^{44,g}, T. Hussain⁷⁰, N. Hüsken^{26,33}, W. Imoehl²⁶, M. Irshad^{68,55}, J. Jackson²⁶, S. Jaeger⁴, S. Janchiv³⁰, E. Jang⁵², J. H. Jeong⁵², Q. Ji¹, Q. P. Ji¹⁹, X. B. Ji^{1,60}, X. L. Ji^{1,55}, Y. Y. Ji⁴⁷, Z. K. Jia^{68,55}, P. C. Jiang^{44,g}, S. S. Jiang³⁷, X. S. Jiang^{1,55,60}, Y. Jiang⁶⁰, J. B. Jiao⁴⁷, Z. Jiao²², S. Jin⁴⁰, Y. Jin⁶³, M. Q. Jing^{1,60}, T. Johansson⁷², S. Kabana³¹, N. Kalantar-Nayestanaki⁶¹, X. L. Kang⁹, X. S. Kang³⁸, R. Kappert⁶¹, M. Kavatsyuk⁶¹, B. C. Ke⁷⁸, I. K. Keshk⁴, A. Khoukaz⁶⁵, R. Kiuchi¹, R. Kliemt¹³, L. Koch³⁵, O. B. Kolcu^{59A}, B. Kopf⁴, M. Kuemmel⁴, M. Kuessner⁴, A. Kupcs^{42,72}, W. Kühn³⁵, J. J. Lane⁶⁴, J. S. Lange³⁵, P. Larin¹⁸, A. Lavanina²⁵, L. Lavezzi^{71A,71C}, T. T. Lei^{68,k}, Z. H. Lei^{68,55}, H. Leithoff³³, M. Lellmann³³, T. Lenz³³, C. Li⁴¹, C. Li⁴⁵, C. H. Li³⁷, Cheng Li^{68,55}, D. M. Li⁷⁸, F. Li^{1,55}, G. Li¹, H. Li^{68,55}, H. B. Li^{1,60}, H. J. Li¹⁹, H. N. Li^{53,i}, Hui Li⁴¹, J. Q. Li⁴, J. S. Li⁵⁶, J. W. Li⁴⁷, Ke Li¹, L. J. Li^{1,60}, L. K. Li¹, Lei Li³, M. H. Li⁴¹, P. R. Li^{36,j,k}, S. X. Li¹¹, S. Y. Li⁵⁸, T. Li⁴⁷, W. D. Li^{1,60}, W. G. Li¹, X. H. Li^{68,55}, X. L. Li⁴⁷, Xiaoyu Li^{1,60}, Y. G. Li^{44,g}, Z. X. Li¹⁵, Z. Y. Li⁵⁶, C. Liang⁴⁰, H. Liang^{1,60}, H. Liang^{68,55}, H. Liang³², Y. F. Liang⁵¹, Y. T. Liang^{29,60}, G. R. Liao¹⁴, L. Z. Liao⁴⁷, J. Libby²⁵, A. Limphirat⁵⁷, C. X. Lin⁵⁶, D. X. Lin^{29,60}, T. Lin¹, B. J. Liu¹, C. Liu³², C. X. Liu¹, D. Liu^{18,68}, F. H. Liu⁵⁰, Fang Liu¹, Feng Liu⁶, G. M. Liu^{53,i}, H. Liu^{36,j,k}, H. B. Liu¹⁵, H. M. Liu^{1,60}, Huanhuan Liu¹, Huihui Liu²⁰, J. B. Liu^{68,55}, J. L. Liu⁶⁹, J. Y. Liu^{1,60}, K. Liu¹, K. Y. Liu³⁸, Ke Liu²¹, L. Liu^{68,55}, L. C. Liu²¹, Lu Liu⁴¹, M. H. Liu^{11,f}, P. L. Liu¹, Q. Liu⁶⁰, S. B. Liu^{68,55}, T. Liu^{11,f}, W. K. Liu⁴¹, W. M. Liu^{68,55}, X. Liu^{36,j,k}, Y. Liu^{36,j,k}, Y. B. Liu⁴¹, Z. A. Liu^{1,55,60}, Z. Q. Liu⁴⁷, X. C. Lou^{1,55,60}, F. X. Lu⁵⁶, H. J. Lu²², J. G. Lu^{1,55}, X. L. Lu¹, Y. Lu⁷, Y. P. Lu^{1,55}, Z. H. Lu^{1,60}, C. L. Luo³⁹, M. X. Luo⁷⁷, T. Luo^{11,f}, X. L. Luo^{1,55}, X. R. Lyu⁶⁰, Y. F. Lyu⁴¹, F. C. Ma³⁸, H. L. Ma¹, L. L. Ma⁴⁷, M. M. Ma^{1,60}, Q. M. Ma¹, R. Q. Ma^{1,60}, R. T. Ma⁶⁰, X. Y. Ma^{1,55}, Y. Ma^{44,g}, F. E. Maas¹⁸, M. Maggiora^{71A,71C}, S. Maldaner⁴, S. Malde⁶⁶, Q. A. Malik⁷⁰, A. Mangoni^{27B}, Y. J. Mao^{44,g}, Z. P. Mao¹, S. Marcelllo^{71A,71C}, Z. X. Meng⁶³, J. G. Messchendorp^{13,61}, G. Mezzadri^{28A}, H. Miao^{1,60}, T. J. Min⁴⁰, R. E. Mitchell²⁶, X. H. Mo^{1,55,60}, N. Yu. Muchnoi^{12,b}, Y. Nefedov³⁴, F. Nerling^{18,d}, I. B. Nikolaev^{12,b}, Z. Ning^{1,55}, S. Nisar^{10,l}, Y. Niu⁴⁷, S. L. Olsen⁶⁰, Q. Ouyang^{1,55,60}, S. Pacetti^{27B,27C}, X. Pan⁵², Y. Pan⁵⁴, A. Pathak³², Y. P. Pei^{68,55}, M. Pelizaeus⁴, H. P. Peng^{68,55}, K. Peters^{13,d}, J. L. Ping³⁹, R. G. Ping^{1,60}, S. Plura³³, S. Pogodin³⁴, V. Prasad^{68,55}, F. Z. Qi¹, H. Qi^{68,55}, H. R. Qi⁵⁸, M. Qi⁴⁰, T. Y. Qi^{11,f}, S. Qian^{1,55}, W. B. Qian⁶⁰, Z. Qian⁵⁶, C. F. Qiao⁶⁰, J. J. Qin⁶⁹, L. Q. Qin¹⁴, X. P. Qin^{11,f}, X. S. Qin⁴⁷, Z. H. Qin^{1,55}, J. F. Qiu¹, S. Q. Qu⁵⁸, K. H. Rashid⁷⁰, C. F. Redmer³³, K. J. Ren³⁷, A. Rivetti^{71C}, V. Rodin⁶¹, M. Rolo^{71C}, G. Rong^{1,60}, Ch. Rosner¹⁸, S. N. Ruan⁴¹, A. Sarantsev^{34,c}, Y. Schelhaas³³, C. Schnier⁴, K. Schoenning⁷², M. Scodeggio^{28A,28B}, K. Y. Shan^{11,f}, W. Shan²³, X. Y. Shan^{68,55}, J. F. Shangguan⁵², L. G. Shao^{1,60}, M. Shao^{68,55}, C. P. Shen^{11,f}, H. F. Shen^{1,60}, W. H. Shen⁶⁰, X. Y. Shen^{1,60}, B. A. Shi⁶⁰, H. C. Shi^{68,55}, J. Y. Shi¹, q. q. Shi⁵², R. S. Shi^{1,60}, X. Shi^{1,55}, J. J. Song¹⁹, W. M. Song^{32,1}, Y. X. Song^{44,g}, S. Sosio^{71A,71C}, S. Spataro^{71A,71C}, F. Stieler³³, P. P. Su⁵², Y. J. Su⁶⁰, G. X. Sun¹, H. Sun⁶⁰, H. K. Sun¹, J. F. Sun¹⁹, L. Sun⁷³, S. S. Sun^{1,60}, T. Sun^{1,60}, W. Y. Sun³², Y. J. Sun^{68,55}, Y. Z. Sun¹, Z. T. Sun⁴⁷, Y. X. Tan^{68,55}, C. J. Tang⁵¹, G. Y. Tang¹, J. Tang⁵⁶, L. Y. Tao⁶⁹, Q. T. Tao^{24,h}, M. Tat⁶⁶, J. X. Teng^{68,55}, V. Thoren⁷², W. H. Tian⁴⁹, Y. Tian^{29,60}, I. Uman^{59B}, B. Wang^{68,55}, B. Wang¹, B. L. Wang⁶⁰, C. W. Wang⁴⁰, D. Y. Wang^{44,g}, F. Wang⁶⁹, H. J. Wang^{36,j,k}, H. P. Wang^{1,60}, K. Wang^{1,55}, L. L. Wang¹, M. Wang⁴⁷, Meng Wang^{1,60}, S. Wang^{11,f}, S. Wang¹⁴, T. Wang^{11,f}, T. J. Wang⁴¹, W. Wang⁵⁶, W. H. Wang⁷³, W. P. Wang^{68,55}, X. Wang^{44,g}, X. F. Wang^{36,j,k}, X. L. Wang^{11,f}, Y. Wang⁵⁸, Y. D. Wang⁴³, Y. F. Wang^{1,55,60}, Y. H. Wang⁴⁵, Y. Q. Wang¹, Yaqian Wang^{17,1}, Z. Wang^{1,55}, Z. Y. Wang^{1,60}, Ziyi Wang⁶⁰, D. H. Wei¹⁴, F. Weidner⁶⁵, S. P. Wen¹, D. J. White⁶⁴, U. Wiedner⁴, G. Wilkinson⁶⁶, M. Wolke⁷², L. Wollenberg⁴, J. F. Wu^{1,60}, L. H. Wu¹, L. J. Wu^{1,60}, X. Wu^{11,f}, X. H. Wu³², Y. Wu⁶⁸, Y. J. Wu²⁹, Z. Wu^{1,55}, L. Xia^{68,55}, T. Xiang^{44,g}, D. Xiao^{36,j,k}, G. Y. Xiao⁴⁰, H. Xiao^{11,f}, S. Y. Xiao¹, Y. L. Xiao^{11,f}, Z. J. Xiao³⁹, C. Xie⁴⁰, X. H. Xie^{44,g}, Y. Xie⁴⁷, Y. G. Xie^{1,55}, Y. H. Xie⁶, Z. P. Xie^{68,55}, T. Y. Xing^{1,60}, C. F. Xu^{1,60}, C. J. Xu⁵⁶, G. F. Xu¹, H. Y. Xu⁶³, Q. J. Xu¹⁶, X. P. Xu⁵², Y. C. Xu⁷⁵, Z. P. Xu⁴⁰, F. Yan^{11,f}, L. Yan^{11,f}, W. B. Yan^{68,55}, W. C. Yan⁷⁸, H. J. Yang^{48,e}, H. L. Yang³², H. X. Yang¹, Tao Yang¹, Y. F. Yang⁴¹, Y. X. Yang^{1,60}, Yifan Yang^{1,60}, M. Ye^{1,55}, M. H. Ye⁸, J. H. Yin¹, Z. Y. You⁵⁶, B. X. Yu^{1,55,60}, C. X. Yu⁴¹, G. Yu^{1,60}, T. Yu⁶⁹, X. D. Yu^{44,g}, C. Z. Yuan^{1,60}, L. Yuan², S. C. Yuan¹, X. Q. Yuan¹, Y. Yuan^{1,60}, Z. Y. Yuan⁵⁶, C. X. Yue³⁷, A. A. Zafar⁷⁰, F. R. Zeng⁴⁷, X. Zeng⁶, Y. Zeng^{24,h}, X. Y. Zhai³², Y. H. Zhan⁵⁶, A. Q. Zhang^{1,60}, B. L. Zhang^{1,60}, B. X. Zhang¹, D. H. Zhang⁴¹, G. Y. Zhang¹⁹, H. Zhang⁶⁸, H. H. Zhang³², H. H. Zhang⁵⁶, H. Q. Zhang^{1,55,60}, H. Y. Zhang⁴⁹, J. J. Zhang⁴⁹, J. L. Zhang⁷⁴, J. Q. Zhang³⁹, J. W. Zhang^{1,55,60}, J. X. Zhang^{36,j,k}, J. Y. Zhang¹, J. Z. Zhang^{1,60}, Jianyu Zhang^{1,60}, Jiawei Zhang^{1,60},

L. M. Zhang⁵⁸, L. Q. Zhang⁵⁶, Lei Zhang⁴⁰, P. Zhang¹, Q. Y. Zhang^{37,78}, Shuihan Zhang^{1,60}, Shulei Zhang^{24,h}, X. D. Zhang⁴³, X. M. Zhang¹, X. Y. Zhang⁴⁷, X. Y. Zhang⁵², Y. Zhang⁶⁶, Y. T. Zhang⁷⁸, Y. H. Zhang^{1,55}, Yan Zhang^{68,55}, Yao Zhang¹, Z. H. Zhang¹, Z. L. Zhang³², Z. Y. Zhang⁷³, Z. Y. Zhang⁴¹, G. Zhao¹, J. Zhao³⁷, J. Y. Zhao^{1,60}, J. Z. Zhao^{1,55}, Lei Zhao^{68,55}, Ling Zhao¹, M. G. Zhao⁴¹, S. J. Zhao⁷⁸, Y. B. Zhao^{1,55}, Y. X. Zhao^{29,60}, Z. G. Zhao^{68,55}, A. Zhemchugov^{34,a}, B. Zheng⁶⁹, J. P. Zheng^{1,55}, Y. H. Zheng⁶⁰, B. Zhong³⁹, C. Zhong⁶⁹, X. Zhong⁵⁶, H. Zhou⁴⁷, L. P. Zhou^{1,60}, X. Zhou⁷³, X. K. Zhou⁶⁰, X. R. Zhou^{68,55}, X. Y. Zhou³⁷, Y. Z. Zhou^{11,f}, J. Zhu⁴¹, K. Zhu¹, K. J. Zhu^{1,55,60}, L. X. Zhu⁶⁰, S. H. Zhu⁶⁷, S. Q. Zhu⁴⁰, W. J. Zhu^{11,f}, Y. C. Zhu^{68,55}, Z. A. Zhu^{1,60}, J. H. Zou¹, J. Zu^{68,55}

(BESIII Collaboration)

- ¹ Institute of High Energy Physics, Beijing 100049, People's Republic of China
² Beihang University, Beijing 100191, People's Republic of China
³ Beijing Institute of Petrochemical Technology, Beijing 102617, People's Republic of China
⁴ Bochum Ruhr-University, D-44780 Bochum, Germany
⁵ Carnegie Mellon University, Pittsburgh, Pennsylvania 15213, USA
⁶ Central China Normal University, Wuhan 430079, People's Republic of China
⁷ Central South University, Changsha 410083, People's Republic of China
⁸ China Center of Advanced Science and Technology, Beijing 100190, People's Republic of China
⁹ China University of Geosciences, Wuhan 430074, People's Republic of China
¹⁰ COMSATS University Islamabad, Lahore Campus, Defence Road, Off Raiwind Road, 54000 Lahore, Pakistan
¹¹ Fudan University, Shanghai 200433, People's Republic of China
¹² G.I. Budker Institute of Nuclear Physics SB RAS (BINP), Novosibirsk 630090, Russia
¹³ GSI Helmholtzcentre for Heavy Ion Research GmbH, D-64291 Darmstadt, Germany
¹⁴ Guangxi Normal University, Guilin 541004, People's Republic of China
¹⁵ Guangxi University, Nanning 530004, People's Republic of China
¹⁶ Hangzhou Normal University, Hangzhou 310036, People's Republic of China
¹⁷ Hebei University, Baoding 071002, People's Republic of China
¹⁸ Helmholtz Institute Mainz, Staudinger Weg 18, D-55099 Mainz, Germany
¹⁹ Henan Normal University, Xinxiang 453007, People's Republic of China
²⁰ Henan University of Science and Technology, Luoyang 471003, People's Republic of China
²¹ Henan University of Technology, Zhengzhou 450001, People's Republic of China
²² Huangshan College, Huangshan 245000, People's Republic of China
²³ Hunan Normal University, Changsha 410081, People's Republic of China
²⁴ Hunan University, Changsha 410082, People's Republic of China
²⁵ Indian Institute of Technology Madras, Chennai 600036, India
²⁶ Indiana University, Bloomington, Indiana 47405, USA
²⁷ INFN Laboratori Nazionali di Frascati, (A)INFN Laboratori Nazionali di Frascati, I-00044, Frascati, Italy; (B)INFN Sezione di Perugia, I-06100, Perugia, Italy; (C)University of Perugia, I-06100, Perugia, Italy
²⁸ INFN Sezione di Ferrara, (A)INFN Sezione di Ferrara, I-44122, Ferrara, Italy; (B)University of Ferrara, I-44122, Ferrara, Italy
²⁹ Institute of Modern Physics, Lanzhou 730000, People's Republic of China
³⁰ Institute of Physics and Technology, Peace Avenue 54B, Ulaanbaatar 13330, Mongolia
³¹ Instituto de Alta Investigación, Universidad de Tarapacá, Casilla 7D, Arica, Chile
³² Jilin University, Changchun 130012, People's Republic of China
³³ Johannes Gutenberg University of Mainz, Johann-Joachim-Becher-Weg 45, D-55099 Mainz, Germany
³⁴ Joint Institute for Nuclear Research, 141980 Dubna, Moscow region, Russia
³⁵ Justus-Liebig-Universität Giessen, II. Physikalisches Institut, Heinrich-Buff-Ring 16, D-35392 Giessen, Germany
³⁶ Lanzhou University, Lanzhou 730000, People's Republic of China
³⁷ Liaoning Normal University, Dalian 116029, People's Republic of China
³⁸ Liaoning University, Shenyang 110036, People's Republic of China
³⁹ Nanjing Normal University, Nanjing 210023, People's Republic of China
⁴⁰ Nanjing University, Nanjing 210093, People's Republic of China
⁴¹ Nankai University, Tianjin 300071, People's Republic of China
⁴² National Centre for Nuclear Research, Warsaw 02-093, Poland
⁴³ North China Electric Power University, Beijing 102206, People's Republic of China
⁴⁴ Peking University, Beijing 100871, People's Republic of China
⁴⁵ Qufu Normal University, Qufu 273165, People's Republic of China
⁴⁶ Shandong Normal University, Jinan 250014, People's Republic of China
⁴⁷ Shandong University, Jinan 250100, People's Republic of China
⁴⁸ Shanghai Jiao Tong University, Shanghai 200240, People's Republic of China
⁴⁹ Shanxi Normal University, Linfen 041004, People's Republic of China
⁵⁰ Shanxi University, Taiyuan 030006, People's Republic of China
⁵¹ Sichuan University, Chengdu 610064, People's Republic of China
⁵² Soochow University, Suzhou 215006, People's Republic of China

- ⁵³ *South China Normal University, Guangzhou 510006, People's Republic of China*
⁵⁴ *Southeast University, Nanjing 211100, People's Republic of China*
- ⁵⁵ *State Key Laboratory of Particle Detection and Electronics, Beijing 100049, Hefei 230026, People's Republic of China*
⁵⁶ *Sun Yat-Sen University, Guangzhou 510275, People's Republic of China*
- ⁵⁷ *Suranaree University of Technology, University Avenue 111, Nakhon Ratchasima 30000, Thailand*
⁵⁸ *Tsinghua University, Beijing 100084, People's Republic of China*
- ⁵⁹ *Turkish Accelerator Center Particle Factory Group, (A)Istinye University, 34010, Istanbul, Turkey; (B)Near East University, Nicosia, North Cyprus, Mersin 10, Turkey*
- ⁶⁰ *University of Chinese Academy of Sciences, Beijing 100049, People's Republic of China*
⁶¹ *University of Groningen, NL-9747 AA Groningen, The Netherlands*
⁶² *University of Hawaii, Honolulu, Hawaii 96822, USA*
- ⁶³ *University of Jinan, Jinan 250022, People's Republic of China*
- ⁶⁴ *University of Manchester, Oxford Road, Manchester, M13 9PL, United Kingdom*
⁶⁵ *University of Muenster, Wilhelm-Klemm-Strasse 9, 48149 Muenster, Germany*
⁶⁶ *University of Oxford, Keble Road, Oxford OX13RH, United Kingdom*
- ⁶⁷ *University of Science and Technology Liaoning, Anshan 114051, People's Republic of China*
⁶⁸ *University of Science and Technology of China, Hefei 230026, People's Republic of China*
⁶⁹ *University of South China, Hengyang 421001, People's Republic of China*
⁷⁰ *University of the Punjab, Lahore-54590, Pakistan*
- ⁷¹ *University of Turin and INFN, (A)University of Turin, I-10125, Turin, Italy; (B)University of Eastern Piedmont, I-15121, Alessandria, Italy; (C)INFN, I-10125, Turin, Italy*
⁷² *Uppsala University, Box 516, SE-75120 Uppsala, Sweden*
⁷³ *Wuhan University, Wuhan 430072, People's Republic of China*
- ⁷⁴ *Xinyang Normal University, Xinyang 464000, People's Republic of China*
⁷⁵ *Yantai University, Yantai 264005, People's Republic of China*
⁷⁶ *Yunnan University, Kunming 650500, People's Republic of China*
⁷⁷ *Zhejiang University, Hangzhou 310027, People's Republic of China*
⁷⁸ *Zhengzhou University, Zhengzhou 450001, People's Republic of China*
- ^a *Also at the Moscow Institute of Physics and Technology, Moscow 141700, Russia*
^b *Also at the Novosibirsk State University, Novosibirsk, 630090, Russia*
^c *Also at the NRC "Kurchatov Institute", PNPI, 188300, Gatchina, Russia*
^d *Also at Goethe University Frankfurt, 60323 Frankfurt am Main, Germany*
- ^e *Also at Key Laboratory for Particle Physics, Astrophysics and Cosmology, Ministry of Education; Shanghai Key Laboratory for Particle Physics and Cosmology; Institute of Nuclear and Particle Physics, Shanghai 200240, People's Republic of China*
^f *Also at Key Laboratory of Nuclear Physics and Ion-beam Application (MOE) and Institute of Modern Physics, Fudan University, Shanghai 200443, People's Republic of China*
- ^g *Also at State Key Laboratory of Nuclear Physics and Technology, Peking University, Beijing 100871, People's Republic of China*
- ^h *Also at School of Physics and Electronics, Hunan University, Changsha 410082, China*
- ⁱ *Also at Guangdong Provincial Key Laboratory of Nuclear Science, Institute of Quantum Matter, South China Normal University, Guangzhou 510006, China*
- ^j *Also at Frontiers Science Center for Rare Isotopes, Lanzhou University, Lanzhou 730000, People's Republic of China*
^k *Also at Lanzhou Center for Theoretical Physics, Lanzhou University, Lanzhou 730000, People's Republic of China*
^l *Also at the Department of Mathematical Sciences, IBA, Karachi, Pakistan*

Using 7.33 fb^{-1} of e^+e^- collision data collected by the BESIII detector at center-of-mass energies between 4.128 and 4.226 GeV, we observe for the first time the decay $D_s^\pm \rightarrow \omega\pi^\pm\eta$ with a statistical significance of 7.6σ . The measured branching fraction of this decay is $(0.54 \pm 0.12 \pm 0.04)\%$, where the first uncertainty is statistical and the second is systematic.

I. INTRODUCTION

Hints of deviations from the Standard Model have been seen in the measurements of the decays of bottom and charm hadrons. In particular, the ratio $R(D^*) \equiv \mathcal{B}(B \rightarrow D^*\tau^+\nu_\tau)/\mathcal{B}(B \rightarrow D^*\mu^+\nu_\mu) = 0.295 \pm 0.010 \pm 0.010$ provided by the Heavy Flavor Averaging Group [1] differs from the Standard Model prediction 0.258 ± 0.005 by 2.5 standard deviations, showing a possible violation of the

lepton flavor universality (LFU). The \mathcal{B} is defined as the branching fraction (BF). The current data taking at B -factories and LHCb will increase the data sample, hence reducing the statistical uncertainty, while an improvement of the systematic uncertainty is also necessary. The $R(D^*)$ measurement in the LHCb experiment [2, 3] suffers from limited knowledge of the $D_s^+ \rightarrow \pi^+\pi^+\pi^-X$ decay, where X stands for all possible particle combinations, since the decay of $B^0 \rightarrow D^{*-}D_s^+, D_s^+ \rightarrow \pi^+\pi^+\pi^-X$ is the main background for the analysis of

$B^0 \rightarrow D^{*-}\tau^+\nu_\tau, \tau^+ \rightarrow \pi^+\pi^+\pi^-X$. Measurements of the BFs of hadronic D_s^+ decays including at least three charged pions in the final states offer key inputs to improve the precision of $R(D^*)$. This work focuses on the previously unobserved mode $D_s^+ \rightarrow \omega\pi^+\eta$, where we require the decay $\omega \rightarrow \pi^+\pi^-\pi^0$.

In addition, hadronic D_s^\pm decays probe the interplay of short-distance weak decay matrix elements and long-distance QCD effects in charm meson decays. But information is still limited for the D_s^+ case, where a large part of the hadronic BF is still unmeasured [4]. The Cabibbo-favored hadronic D_s^+ decays mediated via a $c \rightarrow sW^+, W^+ \rightarrow u\bar{d}$ transition and producing states with hidden strangeness have relatively large BFs. According to Particle Data Group (PDG) [5], the missing hadronic decays of D_s^+ with ω (η) in the final state contribute a fraction of $(1.5 \pm 1.6)\%$ ($(3.0 \pm 3.1)\%$). Among them, the $D_s^+ \rightarrow \omega\pi^+\eta$ decay is predicted to have a relatively large decay rate [6]. The CLEO collaboration [7] claimed evidence for this mode with $\mathcal{B}(D_s^+ \rightarrow \omega\pi^+\eta) = (0.85 \pm 0.54_{\text{stat.}} \pm 0.06_{\text{syst.}})\%$, based on 4.9 ± 2.9 signal events using 0.586 fb^{-1} of e^+e^- collision data taken at the center-of-mass energy $\sqrt{s} = 4.17 \text{ GeV}$. In this paper, we present the first observation and the BF measurement of $D_s^+ \rightarrow \omega\pi^+\eta$ decay using 7.33 fb^{-1} of e^+e^- collision data collected with the BESIII detector between $\sqrt{s} = 4.128$ and 4.226 GeV . Charge conjugate states are implied throughout this paper.

II. DETECTOR AND DATA SETS

The BESIII detector [8] records symmetric e^+e^- collisions provided by the BEPCII storage ring [9], in center-of-mass energies range from 2.0 to 4.95 GeV, with a peak luminosity of $1 \times 10^{33} \text{ cm}^{-2}\text{s}^{-1}$ achieved at center-of-mass energy of 3.77 GeV. The cylindrical core of the BESIII detector covers 93% of the full solid angle and consists of a helium-based multilayer drift chamber (MDC), a plastic scintillator time-of-flight system (TOF), and a CsI(Tl) electromagnetic calorimeter (EMC), which are all enclosed in a superconducting solenoidal magnet providing a 1.0 T magnetic field [10]. The solenoid is supported by an octagonal flux-return yoke with resistive plate counter muon identification modules interleaved with steel. The charged-particle momentum resolution at 1 GeV/c is 0.5%, and the dE/dx resolution is 6% for electrons from Bhabha scattering. The EMC measures photon energies with a resolution of 2.5% (5%) at 1 GeV in the barrel (end cap) region. The time resolution in the TOF barrel region is 68 ps, while that in the end cap region is 110 ps. The end cap TOF system was upgraded in 2015 using multi-gap resistive plate chamber technology, providing a time resolution of 60 ps [11]. About 84% of the data in this analysis benefits from the upgrade.

The data samples are organized into four groups, $\sqrt{s} = 4.128$ and 4.157 GeV , 4.178 GeV , four energies from 4.189 - 4.219 GeV , and 4.226 GeV , acquired during the

same year under consistent running conditions. The integrated luminosities at each energy are given in Table I. Since the cross section of $e^+e^- \rightarrow D_s^{*\pm}D_s^\mp$ production in e^+e^- annihilation is about twenty times larger than the $e^+e^- \rightarrow D_s^+D_s^-$ one [14], the signal events discussed in this paper are selected from the process $e^+e^- \rightarrow D_s^{*\pm}D_s^\mp$.

TABLE I. The integrated luminosities (\mathcal{L}_{int}) and the requirements on M_{rec} for various center-of-mass energies. The definition of M_{rec} is given in Eq. (5). The first and second uncertainties are statistical and systematic, respectively.

\sqrt{s} (GeV) [12]	\mathcal{L}_{int} (pb^{-1}) [13]	M_{rec} (GeV/c^2)
4.128	401.5	[2.060, 2.150]
4.157	408.7	[2.054, 2.170]
4.178	$3189.0 \pm 0.2 \pm 31.9$	[2.050, 2.180]
4.189	$570.0 \pm 0.1 \pm 2.2$	[2.048, 2.190]
4.199	$526.0 \pm 0.1 \pm 2.1$	[2.046, 2.200]
4.209	$572.1 \pm 0.1 \pm 1.8$	[2.044, 2.210]
4.219	$569.2 \pm 0.1 \pm 1.8$	[2.042, 2.220]
4.226	$1100.9 \pm 0.1 \pm 7.0$	[2.040, 2.220]

Inclusive Monte Carlo (MC) samples, 40 times larger than the data sets, are produced between $\sqrt{s} = 4.128$ and 4.226 GeV with a GEANT4-based [15] toolkit, which includes the geometric description of the BESIII detector and the detector response. These samples are used to determine the detection efficiencies and to estimate backgrounds. The samples include the production of open charm processes, the initial-state radiation production of vector charmonium(-like) states and the continuum processes incorporated in KKMC [16, 17]. All particle decays are modelled with EVTGEN [18, 19] using BFs either reported by the PDG [5], when available, or otherwise estimated with LUNDCHARM [20, 21]. Final state radiation from charged final state particles is incorporated using PHOTOS [22]. The signal detection efficiencies and signal shapes are obtained with the signal MC samples. The signal decay $D_s^+ \rightarrow \omega\pi^+\eta$ is generated with a phase-space distribution. The MC samples of the decays $D_s^+ \rightarrow \omega a_0(980)^+$ and $D_s^+ \rightarrow \eta b_1(1235)^+$, used to estimate the systematic uncertainty of MC models, are generated with the SVS model, which describes the decay of a scalar meson to vector plus scalar mesons [18, 19].

III. METHODOLOGY

The data samples were collected just above the $D_s^{*\pm}D_s^\mp$ threshold, such that the $D_s^{*\pm}D_s^\mp$ system is produced exclusively, without any additional hadrons. The tag method [23] was used, which allows to select clean signal samples, providing the opportunity to measure the absolute BFs of the hadronic D_s^+ meson decays. In the tag method, a single-tag (ST) candidate requires only one of the D_s^\pm mesons to be reconstructed via a hadronic decay. In a double-tag (DT) candidate, both the D_s^+ and D_s^- mesons are reconstructed, with the D_s^+ meson decaying to the signal mode $D_s^+ \rightarrow \omega\pi^+\eta$ and the D_s^- meson

decaying to one of the tag modes. The decays $D_s^- \rightarrow K_S^0 K^-$, $D_s^- \rightarrow K^+ K^- \pi^-$ and $D_s^- \rightarrow K^+ K^- \pi^- \pi^0$ are chosen as tag modes, based on the optimization of the figure of merit for DT yields, defined as $S/\sqrt{S+B}$. Here, S and B denote the signal and background yields estimated by the inclusive MC samples, respectively.

To measure the BF, we start from the following equations. The ST yield for each tag mode is given by

$$N^{\text{ST}} = 2N_{D_s^+ D_s^-} \mathcal{B}_{\text{tag}} \epsilon_{\text{tag}}^{\text{ST}}, \quad (1)$$

and the DT yield is given by

$$N^{\text{DT}} = 2N_{D_s^+ D_s^-} \mathcal{B}_{\text{tag}} \mathcal{B}_{\text{sig}} \epsilon_{\text{tag, sig}}^{\text{DT}}, \quad (2)$$

where $N_{D_s^+ D_s^-}$ is the total number of $D_s^{\pm} D_s^{\mp}$ pairs produced in the e^+e^- collisions, \mathcal{B}_{tag} and \mathcal{B}_{sig} are the BFs of the tag and signal modes, respectively, $\epsilon_{\text{tag}}^{\text{ST}}$ is the ST efficiency to reconstruct the tag mode, and $\epsilon_{\text{tag, sig}}^{\text{DT}}$ is the DT efficiency to reconstruct both the tag and signal decay modes. The total DT yield for all the tag modes α and all the sample groups i is written as

$$N_{\text{total}}^{\text{DT}} = \sum_{\alpha, i} N_{\alpha, \text{sig}, i}^{\text{DT}} = \mathcal{B}_{\text{sig}} \sum_{\alpha, i} 2N_{D_s^+ D_s^-}^i \mathcal{B}_{\alpha} \epsilon_{\alpha, \text{sig}, i}^{\text{DT}}. \quad (3)$$

Solving for \mathcal{B}_{sig} ,

$$\mathcal{B}(D_s^+ \rightarrow \omega \pi^+ \eta) = \frac{N_{\text{total}}^{\text{DT}}}{B_{\text{sub}} \sum_{\alpha, i} N_{\alpha, i}^{\text{ST}} \epsilon_{\alpha, \text{sig}, i}^{\text{ST}} / \epsilon_{\alpha, i}^{\text{ST}}}, \quad (4)$$

where the BF $B_{\text{sub}} = \mathcal{B}_{\pi^0 \rightarrow \gamma \gamma} \mathcal{B}_{\eta \rightarrow \gamma \gamma} \mathcal{B}_{\omega \rightarrow \pi^+ \pi^- \pi^0}$ is introduced to take into account that the signal is reconstructed through these decays. The ST yields $N_{\alpha, i}^{\text{ST}}$ and ST efficiencies $\epsilon_{\alpha, i}^{\text{ST}}$ are obtained from the data and inclusive MC samples, respectively. For the inclusive MC samples we use the same ST selection criteria and fitting strategy as those used in data analysis, to extract the number of observed ST events by fitting the M_{tag} distributions, as shown in Fig. 1. The efficiencies are computed as the ratio of the number of observed ST (DT) events and the number of generated ST (DT) events in the inclusive MC samples.

IV. EVENT SELECTION

The D_s^{\pm} candidates are constructed from individual π^{\pm} , K^{\pm} , K_S^0 , π^0 , η , and ω candidates, with the following selection criteria.

Charged tracks detected in the MDC are required to be within a polar angle (θ) range of $|\cos\theta| < 0.93$, where θ is defined with respect to the z -axis, which is the symmetry axis of the MDC. For charged tracks not originating from K_S^0 decays, the distance of closest approach to the interaction point (IP) must be less than 10 cm along the z -axis, and less than 1 cm in the transverse plane. Particle identification (PID) for charged tracks combines the measurements of the dE/dx in the MDC and the flight time in the TOF to form likelihoods $\mathcal{L}(h)$ ($h = K, \pi$) for each

hadron h hypothesis. Charged kaons and pions are identified by comparing the likelihoods for the two hypotheses, $\mathcal{L}(K) > \mathcal{L}(\pi)$ and $\mathcal{L}(\pi) > \mathcal{L}(K)$, respectively.

The K_S^0 candidates are selected by looping over all pairs of tracks with opposite charge, whose distances to the IP along the beam direction are less than 20 cm. These two tracks are assumed to be pions without PID criteria applied. These tracks are required to originate from a common vertex and have a $\pi^+ \pi^-$ invariant mass ($M_{\pi^+ \pi^-}$) in the range $[0.487, 0.511]$ GeV/ c^2 , corresponding to about three times the resolution of the detector.

Photon candidates are identified using showers in the EMC. The deposited energy of each shower must be greater than 25 MeV in the barrel region ($|\cos\theta| < 0.80$) and more than 50 MeV in the end cap region ($0.86 < |\cos\theta| < 0.92$). To exclude showers originating from charged tracks, the angle subtended at the IP by the EMC shower and the position of the closest charged track extrapolated to the EMC must be greater than 10 degrees. The difference between the EMC time and the event start time is required to be within $[0, 700]$ ns to suppress electronic noise and showers unrelated to the event.

The π^0 and η candidates are reconstructed from photon pairs with invariant masses in the ranges $[0.115, 0.150]$ GeV/ c^2 and $[0.500, 0.570]$ GeV/ c^2 , respectively. To improve their invariant mass resolutions, we require that at least one photon comes from the barrel region of the EMC. Furthermore, the π^0 candidates are constrained to the known π^0 mass [5] via a kinematic fit to improve their energy and momentum resolution.

In order to remove soft pions from D^{*+} decays, both charged and neutral pion candidates are subjected to an additional momentum cut, $p(\pi) > 100$ MeV/ c .

TABLE II. Requirements on M_{tag} for various tag modes.

Tag mode	Mass window (GeV/ c^2)
$D_s^- \rightarrow K_S^0 K^-$	[1.948, 1.991]
$D_s^- \rightarrow K^+ K^- \pi^-$	[1.950, 1.986]
$D_s^- \rightarrow K^+ K^- \pi^- \pi^0$	[1.947, 1.982]

Three tag modes are used to reconstruct the ST D_s^- candidate, and the selections on the invariant mass (M_{tag}) for each tag mode are listed in Table II. The tag mode $D_s^- \rightarrow K^- K^+ \pi^-$ is mainly from $\phi \pi^-$ or $\bar{K}^{*0}(892)K^-$. Therefore, we require that $M_{K^- K^+} < 1.05$ GeV/ c^2 or $|M_{K^- K^+} - 0.892| < 0.070$ GeV/ c^2 , where $M_{K^- K^+}$ and $M_{K^+ \pi^-}$ are the invariant masses of $K^- K^+$ and $K^+ \pi^-$, respectively. The tag mode $D_s^- \rightarrow K^- K^+ \pi^- \pi^0$ is mainly from $\phi \rho^-$. Therefore, we require $M_{K^- K^+} < 1.05$ GeV/ c^2 and $|M_{\pi^- \pi^0} - 0.775| < 0.150$ GeV/ c^2 , where $M_{K^- K^+}$ and $M_{\pi^- \pi^0}$ are the invariant masses of $K^- K^+$ and $\pi^- \pi^0$. To further suppress backgrounds from non- $D_s^{*\pm} D_s^{\mp}$ processes, a selection on the variable M_{rec} is applied, defined as

$$M_{\text{rec}} = \sqrt{(p_{\text{cm}} - p_{D_s^-})^2}, \quad (5)$$

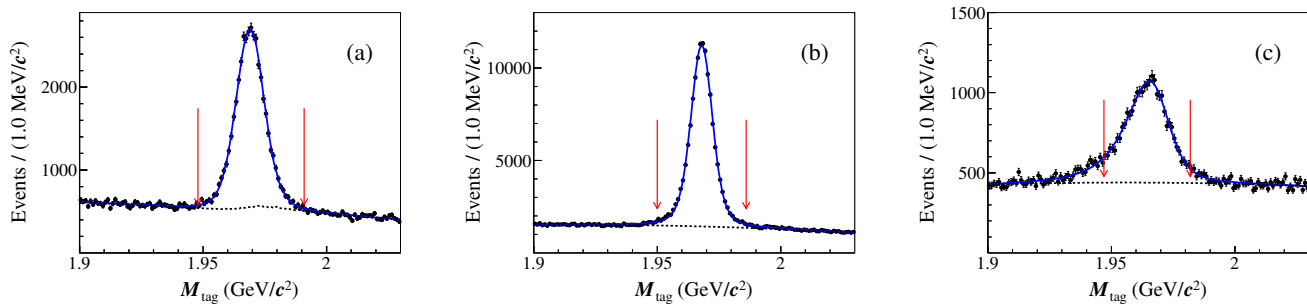


FIG. 1. Fits to the M_{tag} distributions of the ST candidates for (a) $D_s^- \rightarrow K_S^0 K^-$, (b) $D_s^- \rightarrow K^+ K^- \pi^-$ and (c) $D_s^- \rightarrow K^+ K^- \pi^- \pi^0$ from the data sample at $\sqrt{s} = 4.178$ GeV. The points with error bars are data, the blue solid curves are the total fits, and the black dashed curves are the fitted backgrounds. The pairs of red arrows denote the signal regions.

where p_{cm} is the four-momentum of the e^+e^- center-of-mass system, $p_{D_s^-}$ is the four-momentum of the D_s^- candidate in the e^+e^- center-of-mass frame. The mass windows of M_{rec} for D_s^- candidates at various center-of-mass energies are listed in Table I.

For multiple ST candidates, the candidate with M_{rec} closest to the known mass of D_s^{*+} [5] is chosen as the signal candidate. Only 0.16% (0.17%) of events in data (simulated samples) contain multiple D_s^+ candidates, and the multiplicity distribution of the ST candidates shows consistency between data and simulated samples. Table III lists the yields and efficiencies for various tag modes, in which the yields at (I) and (III) are fitted with combined data sets. We use the same ST selection criteria and fitting strategy as those used in data analysis to analyse the inclusive MC samples, and extract the number of observed ST events from fitting the M_{tag} distribution. The ST efficiency is computed as the ratio of the number of observed ST events and the number of generated ST events in the inclusive MC samples. As an example, the fits to the accepted ST candidates from the data sample at $\sqrt{s} = 4.178$ GeV are shown in Fig. 1. In the fits, the signal is modeled by an MC-simulated shape convolved with a Gaussian function taking into account the data-MC resolution difference. The background is described by a second-order Chebyshev polynomial. For the tag mode $D_s^- \rightarrow K_S^0 K^-$, the peaking background from $D^- \rightarrow K_S^0 \pi^-$ is included in the fit, with a shape taken from the inclusive MC samples and its yield floating.

Once a tag mode is identified, we search for the signal decay $D_s^+ \rightarrow \omega \pi^+ \eta$ among the recoiling particles, with the ω and η candidates reconstructed in the $\pi^+ \pi^- \pi^0$ and $\gamma \gamma$ final states, respectively. The $\pi^+ \pi^- \pi^0$ combination with minimum $|M_{\pi^+ \pi^- \pi^0} - m_\omega|$ is used to reconstruct the ω candidates, where m_ω is the known mass of the ω taken from the PDG [5]. The invariant mass distribution of $\pi^+ \pi^- \pi^0$ for data is shown in Fig. 2, in which a clear omega peak is observed. There is no obvious background from $D_s^+ \rightarrow \eta \pi^+ \pi^- \pi^+ \pi^0$ in the ω sideband regions ([0.71, 0.75] and [0.814, 0.854] GeV/c^2). Therefore

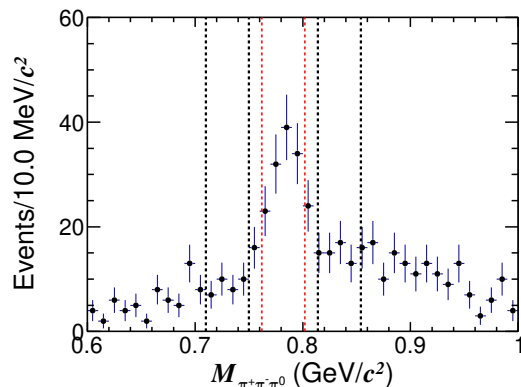


FIG. 2. Invariant mass distribution for selected $\omega \rightarrow \pi^+ \pi^- \pi^0$ candidates at $\sqrt{s} = 4.128 - 4.226$ GeV. The points with error bars are data. The red vertical dashed lines indicate the ω signal region, and the pairs of black dashed lines (left and right of the signal peak) indicate the ω sideband regions.

we require the $\pi^+ \pi^- \pi^0$ invariant mass to be in the omega signal range [0.762, 0.802] GeV/c^2 for further analysis. In the case of multiple candidates, the DT candidate with the average mass, $(M_{\text{sig}} + M_{\text{tag}})/2$, closest to the known D_s^+ mass is retained. The M_{sig} is defined as the invariant-mass of the accepted signal D_s^+ candidates.

To suppress the background from the decay $D_s^+ \rightarrow \pi^+ \pi^0 \eta'$ with $\eta' \rightarrow \pi^+ \pi^- \eta$, we reject candidates with the $\pi^+ \pi^- \eta$ invariant mass less than 1 GeV/c^2 . A kinematic fit is performed under the hypothesis $e^+e^- \rightarrow D_s^{*\pm} D_s^\mp \rightarrow \gamma D_s^+ D_s^-$, with D_s^- decaying to one of the tag modes and D_s^+ decaying to the signal mode. The combination with the minimum χ^2 assuming a D_s^{*+} meson decays to $D_s^+ \gamma$ or a D_s^{*-} meson decays to $D_s^- \gamma$ is chosen to reconstruct the transition photon of $D_s^{*\pm} \rightarrow \gamma D_s^\pm$. To suppress the non- $D_s^{*+} D_s^-$ background, we require the missing energy ($E_{\text{missing}} = E_{\text{cm}} - E_{\text{tag}} - E_{\text{sig}} - E_\gamma$) to be less than 0.08 GeV, where E_{tag} , E_{sig} , and E_γ are the energies of D_s^- , D_s^+ , and transition photon of $D_s^{*\pm} \rightarrow \gamma D_s^\pm$ in the e^+e^- center-of-mass frame, respectively.

TABLE III. The ST yields (N^{ST}) and ST efficiencies (ϵ^{ST}) for the data samples collected at $\sqrt{s} =$ (I) 4.128 and 4.157 GeV, (II) 4.178 GeV, (III) 4.189-4.219 GeV, (IV) 4.226 GeV. The uncertainties are statistical.

Data sample	(I)		(II)		(III)		(IV)	
Tag mode	N^{ST}	ϵ^{ST} (%)	N^{ST}	ϵ^{ST} (%)	N^{ST}	ϵ^{ST} (%)	N^{ST}	ϵ^{ST} (%)
$D_s^- \rightarrow K_S^0 K^-$	6728±144	47.66±0.17	31957±314	47.40±0.08	19960±270	47.20±0.09	6836±163	47.92±0.18
$D_s^- \rightarrow K^+ K^- \pi^-$	23443±202	33.67±0.05	114890±447	32.88±0.02	72827±369	32.69±0.03	24862±227	33.03±0.05
$D_s^- \rightarrow K^+ K^- \pi^- \pi^0$	2414±102	3.43±0.02	13304±269	3.59±0.01	8586±227	3.70±0.02	3172±146	3.84±0.03

V. BRANCHING FRACTION MEASUREMENT

The distributions of the signal D_s^+ candidate invariant mass (M_{sig}), the $\gamma\gamma$ invariant mass ($M_{\gamma\gamma}$), and their two-dimensional scatter plot are shown in Figs. 3 (a), (b), and (c), respectively. It is possible to distinguish three kinds of background events. The events which contain η in final states are called $B_{\eta X}$; they are peaking in $M_{\gamma\gamma}$ but flat in M_{sig} . The events from $D_s^+ \rightarrow \pi^0 \pi^0 \pi^+ \pi^+ \pi^-$, similar to the signal with an incorrectly reconstructed η , are called $B_{3\pi 2\pi^0}$; they are peaking in M_{sig} and flat in $M_{\gamma\gamma}$. The remaining background events are called B_{other} .

The signal yield is extracted from a two-dimensional (2D) unbinned maximum-likelihood fit to the distributions of M_{sig} and $M_{\gamma\gamma}$ at all energy points. The signal shape is described by an MC-simulated 2D probability density function (PDF) convolved with a Gaussian function, whose parameters are derived from the corresponding M_{sig} and $M_{\gamma\gamma}$ fits, to consider resolution the difference between data and MC simulation. The shapes for various background components are modeled from the inclusive MC samples, where the model for $B_{3\pi 2\pi^0}$ is obtained from the amplitude analyses of the decays $D_s^+ \rightarrow \pi^0 \pi^+ \eta$ ($\eta \rightarrow \pi^0 \pi^+ \pi^-$) [24] and $D_s^+ \rightarrow \pi^0 \pi^0 \pi^+ \pi^+ \pi^-$. The yield of $B_{3\pi 2\pi^0}$ is fixed to 152.9 according to the measured BFs, while the yields of $B_{\eta X}$ and B_{other} are floating parameters in the fit.

From the 2D fit, we obtain 78 ± 16 $D_s^+ \rightarrow \omega \pi^+ \eta$ signal events with a statistical significance of 7.6σ . Along with the DT, the corresponding efficiencies are determined and listed in Table IV. We use the same DT selection criteria as those used in data analysis to analyse the inclusive MC samples, and extract the number of obtained DT events from counting the signal events. The DT efficiency is computed as the ratio of the number of obtained DT events and the number of generated DT events in the inclusive MC samples, the yields at $\sqrt{s} = 4.128$ and 4.157 GeV, and $\sqrt{s} = 4.189 - 4.219$ GeV are obtained with combined data sets. The statistical significance is evaluated using $\sqrt{-2\ln(\mathcal{L}_0/\mathcal{L}_{\text{max}})}$, where \mathcal{L}_{max} is the maximum likelihood of the nominal fit and \mathcal{L}_0 is the likelihood of the fit excluding the signal PDF. With Eq. (4), the BF is measured to be $\mathcal{B}(D_s^+ \rightarrow \omega \pi^+ \eta) = (0.54 \pm 0.12)\%$, where the uncertainty is statistical.

The resulting projections on $M_{\eta\pi^+}$, $M_{\omega\pi^+}$ and $M_{\omega\eta}$, as well as the distribution of $M_{\omega\pi^+}^2$ versus $M_{\eta\pi^+}^2$ for the data in the signal region ($M_{\text{sig}} \in (1.94, 1.99)$ and $M_{\gamma\gamma} \in (0.49, 0.57)$ GeV/ c^2), are shown in Fig. 4. Due to

the limited data sample size, no sub-resonances such as $a_0^+(980)$ or $b_1(1235)^+$ can be identified.

VI. SYSTEMATIC UNCERTAINTY

The different systematic uncertainties in the BF measurement are discussed below; most systematic uncertainties related to the efficiency for reconstructing the tag side cancel due to the DT technique.

- ST yield. The total ST yield of the three tag modes is 328979 ± 2880 , resulting in statistical uncertainty $\sqrt{(2880^2 - 328979)/328979} = 0.3\%$. Here, we only consider the statistical fluctuation related to the background of the tag side which is not correlated with the DT sample directly; hence, 0.3% is assigned as a systematic uncertainty.
- π^\pm tracking and PID efficiencies. The systematic uncertainties in the tracking and PID efficiencies per charged pion are assigned to be 1.0% and 1.0%, respectively, estimated by the control sample $e^+ e^- \rightarrow K^- K^+ \pi^- \pi^+$.
- 2D fit. To estimate the systematic uncertainty related with the signal shape, we observe the change in BF when varying the mean and resolution of the convolving Gaussian function by their corresponding uncertainties. We take the variation of the BF, 1.7%, as the systematic uncertainty. The systematic uncertainty due to the MC-simulated background shape is studied by varying the relative fractions of the backgrounds from $q\bar{q}$ and non- $D_s^{*+} D_s^-$ open charm by $\pm 30\%$ [25], the statistical uncertainty of their cross sections. The largest change of the BF, 0.8%, is taken as the systematic uncertainty. The yield of $D_s^+ \rightarrow \pi^0 \pi^0 \pi^+ \pi^+ \pi^-$ is varied by its uncertainty and the change of the BF of 1.0% is assigned as the systematic uncertainty. The systematic uncertainty due to the signal and background on smooth number is estimated by varying parameter that describing the smoothness of the shape from 1.5 to 2 or 1. The change of the BF, 1.3%, is assigned as the systematic uncertainty. The total systematic uncertainty in the 2D fit is obtained to be 2.5%, by adding systematic uncertainties from all above sources in quadrature.

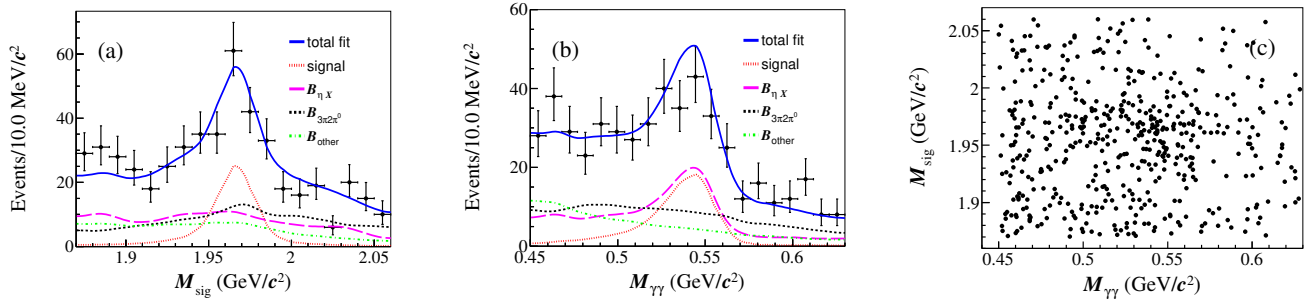


FIG. 3. Distributions of (a) M_{sig} , (b) $M_{\gamma\gamma}$, and (c) M_{sig} versus $M_{\gamma\gamma}$ at $\sqrt{s} = 4.128 - 4.226$ GeV. The points with error bars are data, the solid blue curves are the total fit; other curves show the isolated signal and the individual background contributions from the three labeled sources.

TABLE IV. DT efficiencies (ϵ^{DT}) for the data samples taken at (I) $\sqrt{s} = 4.128$ and 4.157 GeV, (II) $\sqrt{s} = 4.178$ GeV, (III) $\sqrt{s} = 4.189 - 4.219$ GeV, and (IV) $\sqrt{s} = 4.226$ GeV. The BFs of the sub-particle (K_S^0, π^0) decays are not included.

Tag mode	(I) ϵ_{DT} (%)	(II) ϵ_{DT} (%)	(III) ϵ_{DT} (%)	(IV) ϵ_{DT} (%)
$D_s^- \rightarrow K_S^0 K^-$	6.02 ± 0.53	5.96 ± 0.23	5.67 ± 0.28	5.98 ± 0.49
$D_s^- \rightarrow K^+ K^- \pi^-$	4.25 ± 0.20	4.13 ± 0.08	4.06 ± 0.11	3.83 ± 0.17
$D_s^- \rightarrow K^+ K^- \pi^- \pi^0$	0.38 ± 0.06	0.45 ± 0.03	0.43 ± 0.03	0.45 ± 0.06

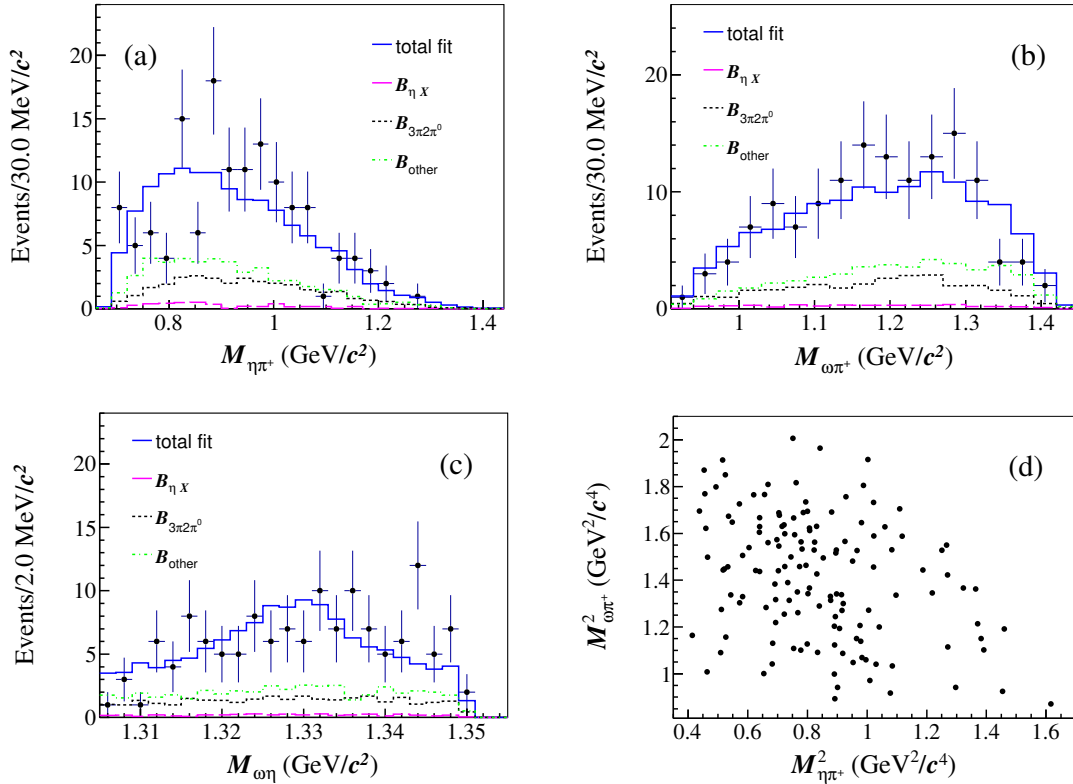


FIG. 4. Mass projections onto (a) $M_{\eta\pi^+}$, (b) $M_{\omega\pi^+}$, (c) $M_{\omega\eta}$ and the distribution of (d) $M_{\omega\pi^+}^2$ versus $M_{\eta\pi^+}^2$ from the combined data sample at $\sqrt{s} = 4.128 - 4.226$ GeV. In (a), (b) and (c), the points with error bars are data and the solid blue curves are the total fit projections; other curves show the individual background contributions from the three labeled sources.

- MC statistics. An uncertainty of 2.3% due to the limited MC statistics is obtained by $\sqrt{\sum_i (f_i \frac{\delta \epsilon_i}{\epsilon_i})^2}$, where f_i is the tag yield fraction, and ϵ_i and $\delta \epsilon_i$ are the signal efficiency and the corresponding uncertainty of tag mode i , respectively.
- π^0 and η reconstruction efficiencies. The systematic uncertainty of the π^0 reconstruction efficiency is estimated to be 2.0% with a control sample of $e^+e^- \rightarrow K^-K^+\pi^-\pi^+\pi^0$. The systematic uncertainty of the η reconstruction efficiency is taken to be 2.0%, based on the π^0 uncertainty. The total systematic uncertainty of 4.0% due to π^0 and η reconstructions is obtained by adding them linearly.
- Quoted BFs. The uncertainties on the quoted BFs of $\pi^0 \rightarrow \gamma\gamma$, $\eta \rightarrow \gamma\gamma$ and $\omega \rightarrow \pi^+\pi^-\pi^0$ are 0.03% (negligible), 0.5% and 0.8%, respectively [5].
- ω mass window. The systematic uncertainty due to the ω mass window is studied by using a control sample of the decay $D^0 \rightarrow K^-\pi^+\omega$. The difference in the efficiencies of the ω mass window between data and MC simulation, 1.2%, is taken as the corresponding systematic uncertainty.
- MC model. To estimate the systematic uncertainty related with the MC model, we separately add $D_s^+ \rightarrow \omega a_0(980)^+$ or $D_s^+ \rightarrow \eta b_1(1235)^+$ signal MC events to inclusive MC samples to improve data-MC consistency (based on agreement of mass projections). The larger change of the signal efficiency, 1.0%, is taken as the related systematic uncertainty.

All of the systematic uncertainties are summarized in Table V. Adding them in quadrature gives a total systematic uncertainty in the BF measurement of 6.6%.

TABLE V. Relative systematic uncertainties of the BF measurement.

Source	Uncertainty (%)
ST yield	0.3
Tracking	3.0
PID	3.0
2D fit	2.5
MC statistics	2.3
π^0 and η reconstruction	4.0
$\mathcal{B}(\eta \rightarrow \gamma\gamma)$	0.5
$\mathcal{B}(\omega \rightarrow \pi^+\pi^-\pi^0)$	0.8
ω mass	1.2
MC model	1.0
Total	7.0

VII. SUMMARY

In summary, using 7.33 fb^{-1} of e^+e^- collision data collected with the BESIII detector between $\sqrt{s} = 4.128$

and 4.226 GeV, we have reported the first observation of $D_s^+ \rightarrow \omega\pi^+\eta$ with a statistical significance of 7.6σ . The absolute BF of this decay is measured to be $\mathcal{B}(D_s^+ \rightarrow \omega\pi^+\eta) = (0.54 \pm 0.12 \pm 0.04)\%$, where the first uncertainty is statistical and the second is systematic. The BF measured in this work is consistent with that of the CLEO collaboration [7], but the precision is improved by a factor of 2.7.

Our result offers an important input for estimating the $D_s^+ \rightarrow \pi^+\pi^+\pi^-X$ background contribution in tests of the LFU with semileptonic B decays. Larger statistics data to be taken in the future [26] will help to search for potential intermediate processes $D_s^+ \rightarrow \omega a_0(980)^+$ and $D_s^+ \rightarrow \eta b_1(1235)^+$.

ACKNOWLEDGMENTS

The BESIII collaboration thanks the staff of BEPCII and the IHEP computing center for their strong support. This work is supported in part by National Key R&D Program of China under Contracts Nos. 2020YFA0406400, 2020YFA0406300; National Natural Science Foundation of China (NSFC) under Contracts Nos. 11635010, 11735014, 11835012, 11935015, 11935016, 11935018, 11961141012, 12022510, 12025502, 12035009, 12035013, 12192260, 12192261, 12192262, 12192263, 12192264, 12192265; the Chinese Academy of Sciences (CAS) Large-Scale Scientific Facility Program; Joint Large-Scale Scientific Facility Funds of the NSFC and CAS under Contract No. U1832207, U1932108; the CAS Center for Excellence in Particle Physics (CCEPP); 100 Talents Program of CAS; The Institute of Nuclear and Particle Physics (INPAC) and Shanghai Key Laboratory for Particle Physics and Cosmology; ERC under Contract No. 758462; European Union's Horizon 2020 research and innovation programme under Marie Skłodowska-Curie grant agreement under Contract No. 894790; German Research Foundation DFG under Contracts Nos. 443159800, 455635585, Collaborative Research Center CRC 1044, FOR5327, GRK 2149; Istituto Nazionale di Fisica Nucleare, Italy; Ministry of Development of Turkey under Contract No. DPT2006K-120470; National Science and Technology fund; National Science Research and Innovation Fund (NSRF) via the Program Management Unit for Human Resources & Institutional Development, Research and Innovation under Contract No. B16F640076; Olle Engkvist Foundation under Contract No. 200-0605; STFC (United Kingdom); Suranaree University of Technology (SUT), Thailand Science Research and Innovation (TSRI), and National Science Research and Innovation Fund (NSRF) under Contract No. 160355; The Royal Society, UK under Contracts Nos. DH140054, DH160214; The Swedish Research Council; U. S. Department of Energy under Contract No. DE-FG02-05ER41374.

-
- [1] Y. S. Amhis *et al.* (HFLAV Collaboration), *Eur. Phys. J. C* **81**, 226 (2021); Updated results available at <https://hflav-eos.web.cern.ch/hflav-eos/semi/spring21/html/RDsDsstar/RDRDs.html>.
- [2] R. Aaij *et al.* (LHCb Collaboration), *Phys. Rev. Lett.* **120**, 171802 (2018).
- [3] R. Aaij *et al.* (LHCb Collaboration), *Phys. Rev. D* **97**, 072013 (2018).
- [4] H. B. Li and X. R. Lyu, *Natl. Sci. Rev.* **8**, nwab181 (2021).
- [5] R. L. Workman *et al.* (Particle Data Group), *Prog. Theor. Exp. Phys.* **2022**, 083C01 (2022).
- [6] M. Gronau and J. L. Rosner, *Phys. Rev. D* **79**, 074022 (2009).
- [7] J. Y. Ge *et al.* (CLEO Collaboration), *Phys. Rev. D* **80**, 051102 (2009).
- [8] M. Ablikim *et al.* (BESIII Collaboration), *Nucl. Instrum. Meth. A* **614**, 345 (2010).
- [9] C. Yu, *et al.* *Proceedings of IPAC2016, Busan, Korea*, 642, 2016.
- [10] K. X. Huang, Z. J. Li, Z. Qian, J. Zhu, H. Y. Li, Y. M. Zhang, S. S. Sun and Z. Y. You, *Nucl. Sci. Tech.* **33**, 142 (2022).
- [11] X. Li *et al.* *Radiat Detect Technol Methods* **1**, 13 (2017); Y.-X. Guo *et al.* *Radiat. Detect. Technol. Methods* **1**, 15 (2017); P. Cao *et al.* *Nucl. Instrum. Meth. A* **953**, 163053 (2020).
- [12] M. Ablikim *et al.* (BESIII Collaboration), *Chin. Phys. C* **45**, 103001 (2021); *Chin. Phys. C* **46**, 113003 (2022).
- [13] M. Ablikim *et al.* (BESIII Collaboration), *Chin. Phys. C* **46**, 113002 (2022). The article described the integrated luminosity measurement for data taken at $\sqrt{s} = 4.189, 4.199, 4.209, 4.219, \text{ and } 4.226$ GeV. The integrated luminosity values for the other data samples have been obtained by a similar procedure.
- [14] D. Cronin-Hennessy *et al.* (CLEO Collaboration), *Phys. Rev. D* **80**, 072001 (2009).
- [15] S. Agostinelli *et al.* (GEANT4 Collaboration), *Nucl. Instrum. Meth. A* **506**, 250 (2003).
- [16] S. Jadach, B. F. L. Ward and Z. Was, *Phys. Rev. D* **63**, 113009 (2001).
- [17] S. Jadach, B. F. L. Ward and Z. Was, *Comput. Phys. Commun.* **130**, 260 (2000).
- [18] D. J. Lange, *Nucl. Instrum. Meth. A* **462**, 152 (2001).
- [19] R. G. Ping, *Chin. Phys. C* **32**, 599 (2008).
- [20] J. C. Chen, G. S. Huang, X. R. Qi, D. H. Zhang and Y. S. Zhu, *Phys. Rev. D* **62**, 034003 (2000).
- [21] R. L. Yang, R. G. Ping and H. Chen, *Chin. Phys. Lett.* **31**, 061301 (2014).
- [22] E. Richter-Was, *Phys. Lett. B* **303**, 163 (1993).
- [23] R. M. Baltrusaitis *et al.* (MARKIII Collaboration), *Phys. Rev. Lett.* **56**, 2140 (1986).
- [24] M. Ablikim *et al.* (BESIII Collaboration), *Phys. Rev. Lett.* **123**, 112001 (2019).
- [25] M. Ablikim *et al.* (BESIII Collaboration), *JHEP* **06**, 181 (2021).
- [26] M. Ablikim *et al.* (BESIII Collaboration), *Chin. Phys. C* **44**, 040001 (2020).